

# An oxadiazole-functionalized ligand and its yellow-emitting Re(I) complex for organoelectronic application

Hu Ge<sup>\*</sup>, Guo Lei, Wei Sheng, Zhang Shuang

College of Chemistry and Chemical Engineering, Chongqing University, Chongqing 400044, China

## ARTICLE INFO

### Article history:

Received 18 January 2012

Accepted 7 February 2012

Available online 18 March 2012

### Keywords:

Re(I) complex

Single crystal

Electroluminescence

Photoluminescence

OLED

## ABSTRACT

A Re(I) complex of  $\text{Re}(\text{CO})_3(\text{PTO})\text{Br}$  with 2-(pyridin-2-yl)-5-p-tolyl-1,3,4-oxadiazole (PTO) as the diamine ligand is synthesized, resulting in a phosphorescent emitter which contains oxadiazole functional moiety. Single crystal analysis confirms that oxadiazole moiety of PTO ligand participates in the coordination with Re center. Coordination ability difference between N atom from pyridine ring and that from oxadiazole moiety is found. Density functional theory calculation on the crystal suggests that the onset electronic transition owns a mixed character of metal-to-ligand-charge-transfer and ligand-to-ligand-charge-transfer. Upon photon excitation,  $\text{Re}(\text{CO})_3(\text{PTO})\text{Br}$  exhibits a yellow emission peaking at 549 nm with a short excited state lifetime of 0.15  $\mu\text{s}$ . Further measurements suggest that  $\text{Re}(\text{CO})_3(\text{PTO})\text{Br}$  owns HOMO and LUMO energy levels of  $-5.79$  V and  $-3.49$  V and a high decomposition temperature of 322 °C. The optimal electroluminescence device using  $\text{Re}(\text{CO})_3(\text{PTO})\text{Br}$  as the emitting dopant shows an orange light of 598 nm, with a maximum luminance of 4600  $\text{cd}/\text{m}^2$  and a maximum current efficiency of 11.5  $\text{cd}/\text{A}$ .

© 2012 Elsevier B.V. All rights reserved.

## 1. Introduction

Owing to their promising advantages over their fluorescence counterparts, phosphorescent transition metal complexes have drawn much research attention for their organoelectronic applications such as organic light-emitting diodes (OLEDs), solar-energy conversion cell, and chemosensors [1,2]. As for OLED application which is generally considered to be a candidate for the next generation flat-display technology, the advantage of using phosphorescent transition metal complex as emissive dopant is that the internal quantum efficiency can theoretically be achieved as high as 100% [3,4]. The effective spin-orbital coupling that exists in transition heavy metal complexes can promote the intersystem crossing from singlet state to triplet state, and thus initiate the radiative decay of triplet excited state. In this case, both singlet and triplet excitons that generated within emitting layer of OLED can be collected by the emissive center, leading to the high internal quantum efficiency [5]. Thus, luminescent metal complexes owing heavy metal cores are highly attractive and desired by OLED researchers.

Phosphorescent Ir(III) complexes have shown promising performance such as high photoluminescence (PL) yield, proper stability and energy levels, short excited state lifetime, and good film-forming ability, making them in general attractive candidates for

OLED application [6]. Further analysis reveals that most Ir(III) based phosphorescent dopants suffer badly from self-quenching at high concentrations, leading to device efficiency decrease at high current density. Doping device structure has been proposed to minimize the concentration-quenching effect, which however makes the device construction process more complicated. The urge for superior phosphorescent emitters without concentration-quenching effect as well as the need for a deeper understanding on the correlation between molecular structure and emitting characteristics has sparked a continuous research for other phosphorescent emitting systems.

Phosphorescent Re(I) complexes then seem to be a challenging candidate owing to the advantages of high thermal and chemical stability, good emission yield, proper energy levels and short excited state lifetimes [6–9]. In addition, most phosphorescent Re(I) complexes own only one emission peak, favoring the desired high color purity for display [8–10]. Adachi and coworkers firstly reported the electroluminescence (EL) from phosphorescent Re(I) complexes, which confirms that they also possess the desired virtues of high PL yield, proper stability and energy levels and so on [7]. Then a series of research interest has been sparked. For example, Zhang, etc. introduce various electron-donor/acceptor groups into the phosphorescent Re(I) complexes ( $\text{Re}(\text{CO})_3(\text{L})\text{Br}$ ,  $\text{L} = 5-(1\text{H-pyrrol-1-yl})-1,10\text{-phenanthroline}$ , 4,5-diazafluorene) to improve the PL and EL performance [8,9]. After a system comparison, it is found that electron-acceptors such as oxadiazole functional group are in the positive position to achieve better PL and EL performance since the functional groups can improve the

\* Corresponding author. Tel./fax: +86 23 65106756.

E-mail address: [cquhuge1@163.com](mailto:cquhuge1@163.com) (G. Hu).

electron transport and thus the charge carrier balance within EL device [10].

Guided by above results, in this effort, we design a Re(I) complex of  $\text{Re}(\text{CO})_3(\text{PTO})\text{Br}$  with 2-(pyridin-2-yl)-5-p-tolyl-1,3,4-oxadiazole (PTO) as the diamine ligand, resulting in a phosphorescent emitter which contains oxadiazole functional moiety. The PL and EL properties of  $\text{Re}(\text{CO})_3(\text{PTO})\text{Br}$  are then studied in detail.

## 2. Experimental details

Scheme 1 shows the synthetic scheme of how to obtain PTO and its corresponding Re(I) complex of  $\text{Re}(\text{CO})_3(\text{PTO})\text{Br}$ . 2-(2H-tetrazol-5-yl)-pyridine (TP) was synthesized according to a literature procedure and used as the starting reagent [11]. The other chemical reagents of 4-methylbenzoyl chloride, sodium azide, zinc bromide,  $\text{Re}(\text{CO})_5\text{Br}$ , 2-cyanopyridine, 4,4',4''-tris[3-methylphenylphenylamino] triphenylamine (referred as *m*-MTDATA), 4,4-bis[*N*-(1-naphthyl)-*N*-phenylamino]biphenyl (NPB), 4,4'-dicarbazolyl-1,1'-biphenyl (CBP), 4,7-diphenyl-1,10-phenanthroline (Bphen), and tris(8-hydroxy-quinoline)aluminum ( $\text{Alq}_3$ ) were purchased from Aldrich Chemical Co. and used as received without further purifications.

### 2.1. Synthesis of PTO ligand and $\text{Re}(\text{CO})_3(\text{PTO})\text{Br}$

#### 2.1.1. PTO

The synthetic route for PTO is described as follows. The mixture of 10 mmol of TP, 11 mmol of 4-methylbenzoyl chloride, and 20 mL of pyridine was brought to reflux under  $\text{N}_2$  atmosphere for 3 days. The mixture was then poured into cold water and filtered. The obtained crude product was purified on a silica gel column (*n*-hexane:ethyl acetate (V:V) = 30:1). Yield: 50%.  $^1\text{H NMR}$  ( $\text{CDCl}_3$ ):  $\delta$  2.47 (3H, s), 7.30 (2H, d,  $J = 6.0$ ), 7.45 (1H, t), 7.92 (1H, t), 8.12 (2H, d,  $J = 6.0$ ), 8.34 (1H, d,  $J = 6.0$ ), 8.84 (1H, d,  $J = 3.6$ ). Anal. Calcd. for  $\text{C}_{14}\text{H}_{11}\text{N}_3\text{O}$ : C, 70.87; H, 4.67; N, 17.71. Found: C, 70.93; H, 4.79; N, 17.56.

#### 2.1.2. $\text{Re}(\text{CO})_3(\text{PTO})\text{Br}$

The synthetic route for  $\text{Re}(\text{CO})_3(\text{PTO})\text{Br}$  is described as follows. The mixture of 0.21 mmol of PTO, 0.20 mmol of  $\text{Re}(\text{CO})_5\text{Br}$ , and 20 mL of toluene was brought to reflux under  $\text{N}_2$  atmosphere for 6 h. After cooling, the solvent was removed by evaporation. The crude product was purified by recrystallization from the mixed solvent of *n*-hexane: $\text{CH}_2\text{Cl}_2 = 1:1$  (V:V). The residue was chromat-

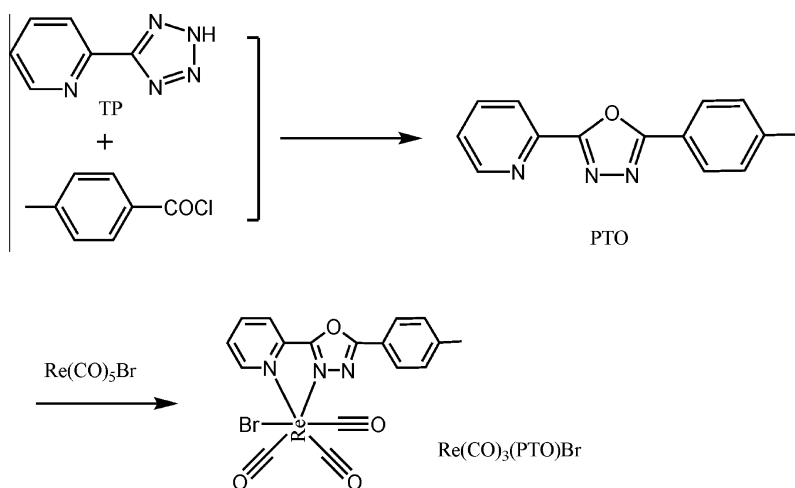
graphed on a silica gel column (*n*-hexane:ethyl acetate (V:V) = 20:1) to give the desired product.  $^1\text{H NMR}$  ( $\text{CDCl}_3$ ):  $\delta$  2.52 (3H, s), 7.43 (2H, d,  $J = 6.0$ ), 7.54 (1H, t), 8.01 (1H, t), 8.19 (2H, d,  $J = 6.0$ ), 8.38 (1H, d,  $J = 6.0$ ), 8.97 (1H, d,  $J = 4.0$ ). Anal. Calcd. for  $\text{C}_{11}\text{H}_{11}\text{BrN}_3\text{O}_4\text{Re}$ : C, 25.64, H, 2.15, N, 8.15. Found: C, 25.74, H, 2.27, N, 8.09. Its identity is further confirmed by single crystal XRD (entry number: CCDC-797507 which can be obtained free of charge from The Cambridge Crystallographic Data Center via <http://www.ccdc.cam.ac.uk/conts/retrieving.html>).

### 2.2. Construction of EL devices

All EL devices were constructed by vacuum deposition method. For a typical run, organic functional layers were deposited in sequence onto pre-cleaned ITO substrates (resistivity  $< 30 \Omega$ , active area =  $4 \text{ mm}^2$ ) by resistive heating method with a chamber pressure of  $\sim 2 \times 10^{-4}$  Pa. EL spectra were recorded with a PR650 spectrascan spectrometer. Device luminance-current density-voltage characteristics were recorded simultaneously with the measurement of EL spectra by combining the spectrometer with a Keithley 2400 source meter.

### 2.3. Methods and measurements

$^1\text{H NMR}$  spectra were obtained from a Varian INOVA 300 spectrometer. X-ray diffraction analysis of  $\text{Re}(\text{CO})_3(\text{PTO})\text{Br}$  was performed on a Siemens P4 single-crystal X-ray diffractometer with a Smart CCD-1000 detector and graphite-monochromated  $\text{Mo K}\alpha$  radiation at room temperature (50 kV, 30 A). All hydrogen atoms of  $\text{Re}(\text{CO})_3(\text{PTO})\text{Br}$  were theoretically calculated. UV-Vis absorption spectra were recorded in dilute solutions using a HP 8453 UV-Vis-NIR diode array spectrophotometer. Photoluminescence and excitation spectra were recorded with a Hitachi F-4500 fluorescence spectrophotometer. Excited state lifetime was obtained with 355 nm light pulsed by Nd:yttrium aluminum garnet (YAG) laser. Thermogravimetric analysis (TGA) data were recorded with a thermal analysis instrument (SDT2960, TA Instruments, New Castle, DE) with a heating rate of  $10 \text{ }^\circ\text{C}/\text{min}$ . Cyclic voltammetry measurements were conducted on a voltammetric analyzer (CH Instruments, Model 620B) with a polished Pt plate as the working electrode, Pt mesh as the counter electrode, and a commercially available saturated calomel electrode (SCE) as the reference electrode, with a scan rate of 0.1 V/s. The voltammograms were recorded in  $\text{CH}_3\text{CN}$  solutions with  $\sim 10^{-3}$  M sample and 0.1 M tetrabutylammonium hexafluorophosphate ( $\text{TBAPF}_6$ ) as the



Scheme 1. A synthetic procedure for PTO and  $\text{Re}(\text{CO})_3(\text{PTO})\text{Br}$ .

supporting electrolyte. Before each electrochemical measurement, the solution was bubbled with nitrogen for 5 min to eliminate the dissolved O<sub>2</sub>. Density functional theory (DFT) and singlet excitation calculations on Re(CO)<sub>3</sub>(PTO)Br were performed at RB3PW91/SBKJC level using its single crystal structure as the initial structure without further geometry optimization [12]. The calculation was finished by GAMESS.

### 3. Results and discussion

#### 3.1. Re(CO)<sub>3</sub>(PTO)Br single crystal analysis

As above mentioned, electron-withdrawing oxadiazole moiety is introduced into Re(CO)<sub>3</sub>(PTO)Br to improve its PL and EL performance. The single crystal of Re(CO)<sub>3</sub>(PTO)Br was obtained successfully, which confirms the successful formation of oxadiazole moiety. From Fig. 1, it can be seen that the free rotation of the σ bond between phenyl and oxadiazole rings makes them coplanar with each other, which is not consistent with literature case [11]. The fine conjugation between phenyl and oxadiazole rings in PTO ligand may be responsible for this phenomenon. The Re(I) center is surrounded by two N atoms from PTO ligand, three C atoms from CO fragment, and one Br atom, forming a typical octahedral coordination environment. The geometric parameters of Re(CO)<sub>3</sub>(PTO)Br listed in Table 1 are similar to literature values of Re(CO)<sub>3</sub>(L)X (L = 1-(4-5'-phenyl-1,3,4-oxadiazolylbenzyl)-2-pyridinylbenzimidazole, 1-(4-carbazolylbutyl)-2-pyridinylbenzimidazole, and 2-(1-ethylbenzimidazol-2-yl)pyridine, X = Cl, Br), owing to the similar coordination environment [10]. It is then found that the bond length value of Re–N(2) is shorter than that of Re–N(1), suggesting that the attraction between Re atom and N atom from oxadiazole moiety is stronger than that between Re atom and N atom from pyridine moiety. It is expected that the coordination ability of N(2) is enhanced by the electronic effect of O and N atoms in oxadiazole moiety. The bite angle of PTO ligand with Re atom, N(1)–Re–N(2), is measured to be 73.25°. This value is obviously smaller than the corresponding value (~80°) in tetrahedral coordination environment owing similar diamine ligand [13]. Except for the atomic radius difference between various coordination center, the roomy coordination sphere in Re(CO)<sub>3</sub>(PTO)Br may also be responsible for the small bite angle of N(1)–Re–N(2), according to the literature report [13,14]. The geometric relaxation of coordination sphere has been proved to be a major

**Table 1**

Selected geometric parameters of Re(CO)<sub>3</sub>(PTO)Br obtained from single crystal.

Bond length	Å	Bond angle	°
Re–C(1)	1.886	N(1)–Re–N(2)	73.25
Re–C(2)	1.920	N(1)–Re–C(2)	91.86
Re–C(3)	1.890	N(2)–Re–C(2)	95.49
Re–Br(1)	2.615	N(1)–Re–Br(1)	86.37
Re–N(1)	2.228	N(2)–Re–Br(1)	84.80
Re–N(2)	2.169	C(1)–Re–Br(1)	92.72
		C(3)–Re–Br(1)	90.27

factor for excited state non-radiative decay. Since the three CO and one Br ligands do not generate any obvious steric hindrances, the geometric relaxation of coordination sphere may be serious. Consequently, the emissive state of Re(CO)<sub>3</sub>(PTO)Br may be compromised by the geometric relaxation, leading to a low emission yield.

#### 3.2. DFT calculation on Re(CO)<sub>3</sub>(PTO)Br

As mentioned before, the phosphorescent emitters surpass the fluorescent counterparts by the fact that they can utilize both singlet and triplet excited state energies. In order to get a clear understanding on the excitation character of Re(CO)<sub>3</sub>(PTO)Br, as well as its frontier molecular orbitals (MOs), a DFT calculation, which is considered to be a reliable method to explore the electronic transition nature of transition metal complexes, is performed on Re(CO)<sub>3</sub>(PTO)Br [13,14]. From the calculation results summarized in Table 2, it can be seen that the first five singlet excitations involve five frontier MOs. The highest occupied molecular orbital (HOMO) and HOMO – 1 of Re(CO)<sub>3</sub>(PTO)Br are mainly composed of contributions from Re and Br atoms. As for HOMO – 2, the contribution from Re atom increases to over 60%, showing an obvious metal character. The composition of the lowest unoccupied molecular orbital (LUMO) and LUMO + 1 of Re(CO)<sub>3</sub>(PTO)Br is much less complicated. As shown in Table 2, LUMO and LUMO + 1 are dominated by contribution from PTO ligand, which means that they are π\* in nature, which is consistent with literature report [13,14]. The first five singlet electronic transitions correspond to electronic transitions from HOMO, HOMO – 1 and HOMO – 2 to LUMO and LUMO + 1. According our analysis on the nature of these MOs, the electronic transitions are thus assigned as a mixed character

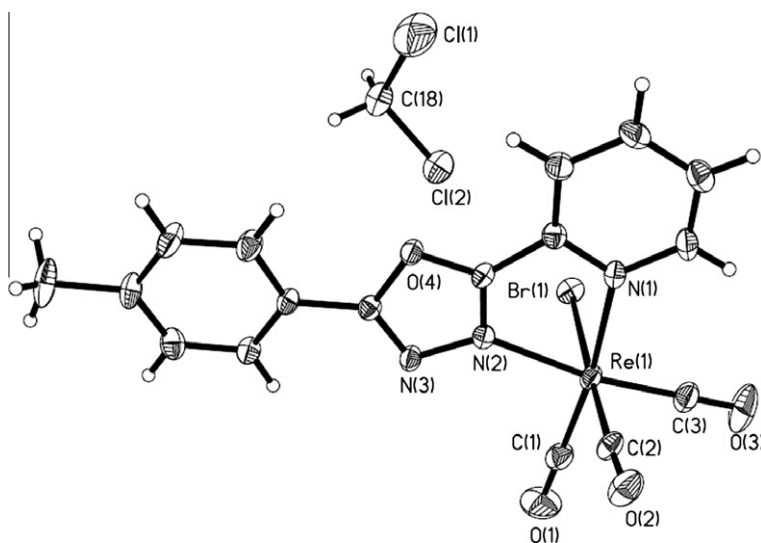


**Fig. 1.** Crystal structure of Re(CO)<sub>3</sub>(PTO)Br.

**Table 2**

Percentage composition of selected molecular orbitals (MOs) and selected singlet excitations calculated at RB3PW91/SBKJC level.

MO/transition	Energy (eV)	Contribution (%)	Character
LUMO + 1(72)	-2.253	Re(1.3)PTO(96.7)CO(1.6)Br(0.4)	PTO
<b>LUMO(71)</b>	-3.099	Re(5.3)PTO(88.8)CO(3.9)Br(2.0)	PTO
<b>HOMO(70)</b>	-5.627	Re(35.5)PTO(4.4)CO(18.2)Br(41.8)	Re/Br
HOMO - 1(69)	-5.747	Re(29.0)PTO(8.9)CO(14.2)Br(48.0)	Re/Br
HOMO - 2(68)	-6.566	Re(61.4)PTO(10.2)CO(27.6)Br(0.7)	Re/CO
S <sub>0</sub> → S <sub>1</sub>	1.775	70 → 71(98.6)	ML/LLCT
S <sub>0</sub> → S <sub>2</sub>	2.004	69 → 71(98.0)	ML/LLCT
S <sub>0</sub> → S <sub>3</sub>	2.656	68 → 71(98.6)	MLCT/ LLCT
S <sub>0</sub> → S <sub>4</sub>	2.734	70 → 72(96.2)	ML/LLCT
S <sub>0</sub> → S <sub>5</sub>	2.854	69 → 72(97.6)	ML/LLCT

of metal-to-ligand-charge-transfer and ligand-to-ligand-charge-transfer [(ML + LL)CT]. Correspondingly, the low energy absorption in visible region of Re(CO)<sub>3</sub>(PTO)Br shown in Fig. 2 can be assigned as the electronic absorption of (ML + LL)CT, which will be discussed and proved below.

### 3.3. Photophysical property of Re(CO)<sub>3</sub>(PTO)Br

#### 3.3.1. Electronic absorption and excitation

In order to get a further understanding on the electronic transition of Re(CO)<sub>3</sub>(PTO)Br, the UV–Vis absorption spectrum of Re(CO)<sub>3</sub>(PTO)Br in CH<sub>2</sub>Cl<sub>2</sub> solutions with a concentration of  $1 \times 10^{-4}$  mol/L is measured and shown in Fig. 2. It can be seen that there are two main components for the absorption spectrum. The first one is the high energy absorption band ranging from 250 nm to 360 nm with multiple peaks. After the comparison with the absorption spectrum of PTO ligand shown in Fig. 2, the high energy absorption characteristics are similar to those of pure PTO ligand, thus the high energy absorption is assigned as ligand  $\pi \rightarrow \pi^*$  transitions. The low energy absorption band of Re(CO)<sub>3</sub>(PTO)Br ranging from 365 nm to 470 nm is a newly-generated compared with the absorption spectrum of free PTO ligand. Our DFT calculation result suggests that this low energy absorption corresponds to the electronic absorption of (ML + LL)CT. It has been reported that a similar Re(I) complex with 1,10-phenanthroline as the diamine ligand shows an absorption edge of  $\sim 500$  nm [8]. Consequently, we come to a conclusion that the introduction of oxadiazole moiety tends to increase the energy required for onset electronic transition, owing to its electron-withdrawing nature. It is also

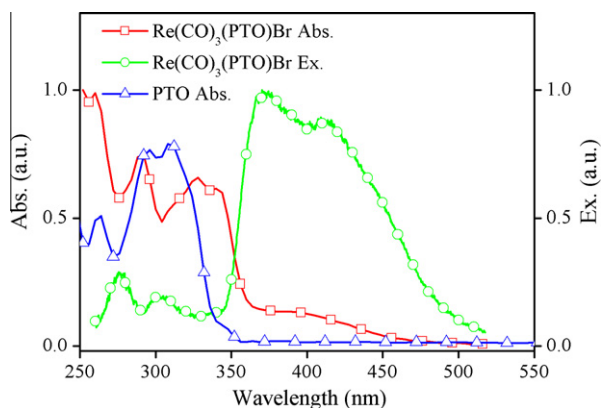


**Fig. 2.** Absorption and excitation spectra of Re(CO)<sub>3</sub>(PTO)Br in CH<sub>2</sub>Cl<sub>2</sub> solutions with a concentration of  $1 \times 10^{-4}$  mol/L, along with the absorption spectrum of free PTO.

expected that the corresponding energy band of Re(CO)<sub>3</sub>(Phen)Br is increased, which means that the energy band of a Re(I) complex can be changed by various diamine ligand.

Even though the molar extinction coefficient of ligand  $\pi \rightarrow \pi^*$  absorption is much higher than that of (ML + LL)CT absorption, the excitation spectrum of Re(CO)<sub>3</sub>(Phen)Br suggests that ligand  $\pi \rightarrow \pi^*$  excitation is ineffective to transfer photon energy to the emissive center, while the electronic excitation of (ML + LL)CT is highly effective on transferring photon energy to the emissive center. This is because the emissive center derives from (ML + LL)CT excited state, and the (ML + LL)CT excitation suffers no non-radiative decay or system crossing, leading to the highly effective excitation. The molar extinction coefficient and energy transfer path differences between ligand  $\pi \rightarrow \pi^*$  excitation and (ML + LL)CT excitation result in the obvious inconsistency between absorption and excitation spectra [15].

#### 3.3.2. Emission spectrum, emission decay dynamics and emission yield

Re(CO)<sub>3</sub>(PTO)Br shows a yellow emission peaking at 549 nm upon 350 nm excitation. The emission spectrum shown in Fig. 3 gives no vibronic progressions with a full width at half maximum (FWHM) of  $\sim 77$  nm, indicating that the charge-transfer nature of the electronic transition. This finding is consistent with above theoretical calculation result. We mentioned that the emissive state of Re(CO)<sub>3</sub>(PTO)Br may be compromised by the geometric relaxation that happens in the excited state. The Stokes shift between absorption edge (470 nm) and emission peak (549 nm) is as large as 79 nm and falls in the literature region of  $\sim 80$  nm [11–14], which means that the geometric relaxation of excited state is indeed remarkable. On the other hand, the FWHM value of Re(CO)<sub>3</sub>(PTO)Br (79 nm) is smaller than that of a typical Re(I) complex of Re(CO)<sub>3</sub>(Phen)Br (90 nm), where Phen = 1,10-phenanthroline [8]. From above data comparison, it is concluded that the electronic effect of oxadiazole moiety suppresses the structural distortion of Re(CO)<sub>3</sub>(PTO)Br excited state, leading to the decreased FWHM value.

The emission decay dynamics is explored by measuring its excited state lifetime as shown as the inset of Fig. 3. The yellow emission of Re(CO)<sub>3</sub>(PTO)Br follows a biexponential decay pattern with  $\tau_1 = 0.074 \mu\text{s}$  ( $A_1 = 2.005$ ) and  $\tau_2 = 0.339 \mu\text{s}$  ( $A_2 = 0.363$ ), respectively. We have observed a successful but inefficient band in  $\pi \rightarrow \pi^*$  excitation region, which means that there is energy transfer from  $\pi \rightarrow \pi^*$  state to the lower (ML + LL)CT state. Consequently, the short-lived decay component of Re(CO)<sub>3</sub>(PTO)Br ( $\tau_1$ ) can be assigned to the radiative decay of  $\pi \rightarrow \pi^*$  excited state, while the long-lived one of  $\tau_2$  is attributed to the MLCT excited state decay. This assignment is consistent with the electronic nature of  $\pi \rightarrow \pi^*$  and MLCT

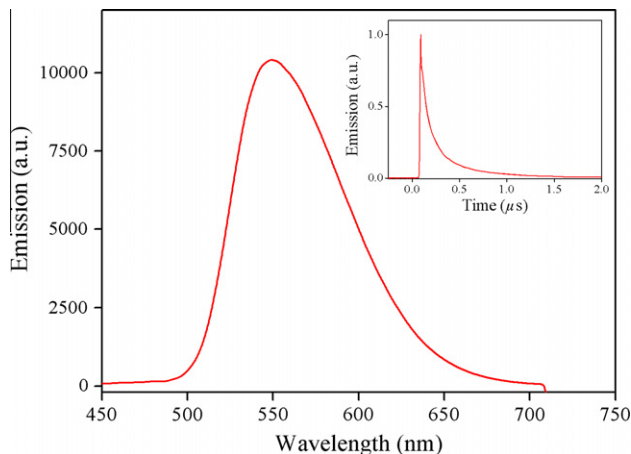


**Fig. 3.** PL spectrum of Re(CO)<sub>3</sub>(PTO)Br in solid state. Inset: PL decay data.

transition. What is more, the long-lived excited state reveals the phosphorescence nature of the yellow emission, favoring the requirement for OLED application.

The emission yield ( $\Phi$ ), which is defined as the ratio of the number of photons emitted to the number of photons absorbed, is measured to be 0.07, using the literature method [15]. This emission yield is not satisfactory enough, and the geometric relaxation that occurs in  $\text{Re}(\text{CO})_3(\text{PTO})\text{Br}$  excited state should be responsible for the unsatisfactory  $\Phi$  of  $\text{Re}(\text{CO})_3(\text{PTO})\text{Br}$  [14]. In order to get a further understanding on the emission dynamics, the radiative probability ( $K_r$ ) and non-radiative probability ( $K_{nr}$ ) are calculated to be  $4.67 \times 10^5 \text{ s}^{-1}$  and  $62.00 \times 10^5 \text{ s}^{-1}$ , respectively, using the following expression [14]:

$$\Phi = \frac{K_r}{K_r + K_{nr}} \quad (1)$$

$$\frac{1}{\tau} = K_r + K_{nr} \quad (2)$$

$K_{nr}$  value is found to be much bigger than that of  $K_r$ , which means that the excited state decay is dominated by the non-radiative decay with the radiative decay process largely suppressed, leading to the low emission yield.

#### 3.4. Energy levels of $\text{Re}(\text{CO})_3(\text{PTO})\text{Br}$

The energy levels of  $\text{Re}(\text{CO})_3(\text{PTO})\text{Br}$  which are critical for EL device design are evaluated by cyclic voltammogram. As shown in Fig. 4, an irreversible metal-centered oxidation wave and a ligand-based reduction wave are observed for  $\text{Re}(\text{CO})_3(\text{PTO})\text{Br}$ , owing to the charge transfer electronic process. The oxidation wave corresponding to  $[\text{Re}^{\text{I}}(\text{CO})_3(\text{PTO})\text{Br}]/[\text{Re}^{\text{II}}(\text{CO})_3(\text{PTO})\text{Br}]$  peaks at +1.27 V with onset oxidation potential ( $V_{\text{onset}}$ ) of +1.05 V. The reduction wave corresponding to  $[\text{Re}^{\text{I}}(\text{CO})_3(\text{PTO})\text{Br}]/[\text{Re}^{\text{I}}(\text{CO})_3(\text{PTO})\text{Br}]^-$  peaks at -1.57 V with onset reduction potential  $V_{\text{onset}}$  of -1.25 V. The HOMO and LUMO energy levels are then calculated to be -5.79 V and -3.49 V with the following formulas, respectively.

$$E_{\text{HOMO}} = -4.74 - E_{\text{onset}}(\text{Ox}) \quad (3)$$

$$E_{\text{LUMO}} = -4.74 - E_{\text{onset}}(\text{Red}) \quad (4)$$

The energy band gap between LUMO and HOMO is calculated to be 2.30 eV, which is slightly narrower than that obtained from optical absorption edge of 2.64 eV (470 nm). The interaction be-

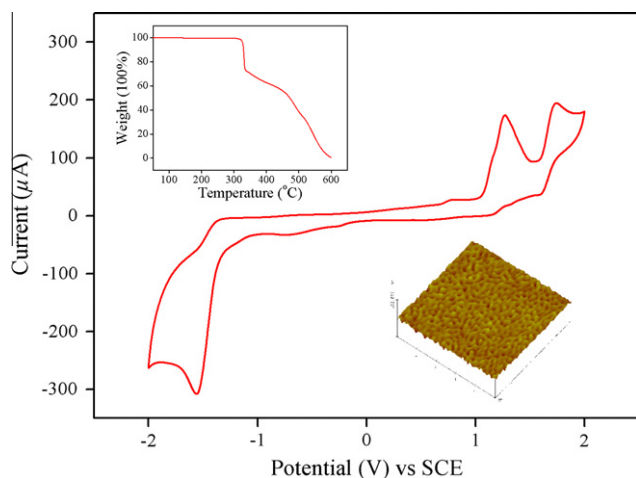


**Fig. 4.** Cyclic voltammogram of  $\text{Re}(\text{CO})_3(\text{PTO})\text{Br}$ . Inset: TGA curve of  $\text{Re}(\text{CO})_3(\text{PTO})\text{Br}$  (up) and the atomic force microscopy image of 10 wt.%  $\text{Re}(\text{CO})_3(\text{PTO})\text{Br}$  doped CBP film (down).

tween  $\text{Re}(\text{CO})_3(\text{PTO})\text{Br}$  and solvent molecules should accelerate the geometric relaxation of  $\text{Re}(\text{CO})_3(\text{PTO})\text{Br}$  and be responsible for this decreased energy band gap [16]. Compared with HOMO and LUMO energy levels of  $\text{Re}(\text{CO})_3(\text{Phen})\text{Br}$  reported by literature ( $E_{\text{HOMO}} = -6.44 \text{ V}$ ,  $E_{\text{LUMO}} = -3.94 \text{ V}$ ) [8], those of  $\text{Re}(\text{CO})_3(\text{PTO})\text{Br}$  are observed to be higher. It is thus concluded that the introduction of oxadiazole moiety as well as the large conjugation rings can increase both HOMO and LUMO energy levels. In addition, the HOMO and LUMO energy levels of  $\text{Re}(\text{CO})_3(\text{PTO})\text{Br}$  fall in the energy gap values of general host materials for OLED application, which means that it is convenient for  $\text{Re}(\text{CO})_3(\text{PTO})\text{Br}$  to take a doping device structure [16,17].

#### 3.5. Thermal durability of $\text{Re}(\text{CO})_3(\text{PTO})\text{Br}$

The thermal character is critical for an emitter since the OLED construction generally experiences a vacuum evaporation procedure. The inset of Fig. 4 indicates that  $\text{Re}(\text{CO})_3(\text{PTO})\text{Br}$  is thermally stable enough until 322 °C, making it thermally stable enough to experience device fabrication through vacuum evaporation. In addition, the atomic force microscopy image of 10 wt.%  $\text{Re}(\text{CO})_3(\text{PTO})\text{Br}$  doped CBP film suggest that the film-forming ability of CBP is some what compromised by the introduction of  $\text{Re}(\text{CO})_3(\text{PTO})\text{Br}$ , owing to the strong polar effect of oxadiazole moiety.

#### 3.6. EL performance of $\text{Re}(\text{CO})_3(\text{PTO})\text{Br}$

$\text{Re}(\text{CO})_3(\text{PTO})\text{Br}$  has shown some promising characters as a phosphorescent dopant for OLED application, such as proper emissive energy and yield, suited energy levels, good thermal stability and film-forming ability. We thus want to further investigate its application in OLEDs. A typical doping device structure of ITO/*m*-MTDATA (30 nm)/NPB (20 nm)/CBP: $\text{Re}(\text{CO})_3(\text{PTO})\text{Br}$  (30 nm)/Bphen (20 nm)/Alq<sub>3</sub> (20 nm)/LiF/Al is used in this effort. *m*-MTDATA is used as a hole-injection layer, NPB acts as a hole-transporting layer, Bphen and Alq<sub>3</sub> are employed as exciton-blocking layer and electron-transporting layer, respectively.

First, we try various dopant concentrations from 5 wt.% to 20 wt.% to optimize the device structure, and the EL spectra are shown in Fig. 5. Upon a low dopant concentration of 5 wt.%, a strong blue emission peaking at 425 nm is observed. Considering that electrons move much faster than holes in OLEDs, the charge carrier recombination must happen in CBP or NPB layers [16,17]. According to a literature report, the CBP emission peaks at ~390 nm [18], the strong blue emission of 425 nm is thus assigned to NPB emission, which means that excess electrons have been injected into the hole-transporting layer, leading to the emission from NPB. Upon higher dopant concentration, more and more

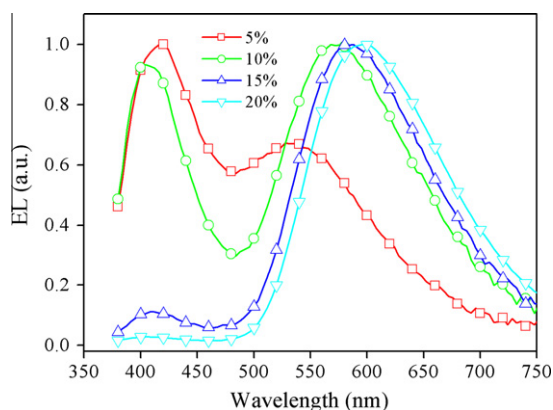


**Fig. 5.** EL spectra of EL devices upon various dopant concentrations at 10 V.

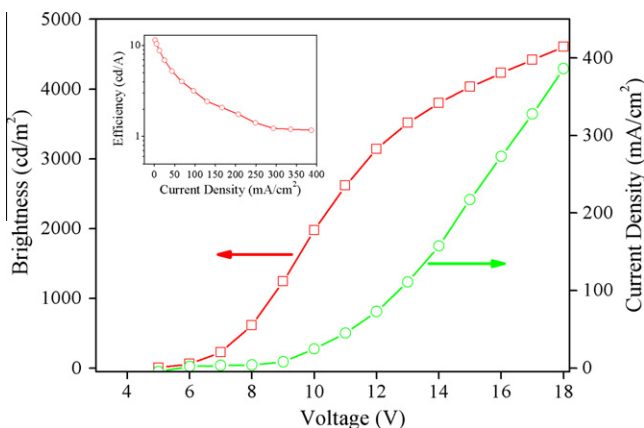


**Fig. 6.** Luminance–current density characteristics of the 20 wt.% doped device upon various voltages. Inset: current efficiency characteristics upon increasing current densities of the 20 wt.% doped device.

electrons are trapped by the emissive center, with the NBP emission largely decreased. The 20 wt.% doped EL device exhibits only characteristics emission from  $\text{Re}(\text{CO})_3(\text{PTO})\text{Br}$  phosphor. An even higher dopant concentration compromises the EL performance by showing unexpected EL emission. The four EL spectra fall in a region from 536 nm to 598 nm with increasing dopant concentrations as shown in Fig. 5. With the increasing dopant concentration, the interaction between emissive molecules is getting stronger, leading to the spectroscopic red<sup>1</sup> shift tendency [17].

Fig. 6 shows the luminance–current density characteristics of the 20 wt.% doped device upon various voltages. A maximum luminance of 4600  $\text{cd}/\text{m}^2$  is achieved with current efficiency of 1.17  $\text{cd}/\text{A}$  and current density of 391  $\text{mA}/\text{cm}^2$ . And a maximum current efficiency of 11.50  $\text{cd}/\text{A}$  is observed at a current density of 1.8  $\text{mA}/\text{cm}^2$  with luminance of 205  $\text{cd}/\text{m}^2$ . The current efficiency characteristics of the 20 wt.% doped device upon increasing current densities shown by the inset of Fig. 6 suggests that the device efficiency decreases obviously with the increasing current density. A short excited state lifetime of emissive center can minimize the triplet–triplet and triplet–polar annihilations and then avoid efficiency roll-off [19]. In other words, the excited state lifetime needs to be further shortened to achieve a high efficiency at high current density. The maximum brightness, however, is not satisfactory enough. Considering the suited energy levels, proper thermal stability and film-forming ability, the low emission yield should be the causation for the low brightness.

Considering the obvious coverage between CBP emission (390 nm) and  $\text{Re}(\text{CO})_3(\text{PTO})\text{Br}$  absorption, it is reasonable to expect a Förster energy transfer path from singlet CBP to (ML + LL)CT excited state of  $\text{Re}(\text{CO})_3(\text{PTO})\text{Br}$ . On the other hand, HOMO and LUMO energy levels of  $\text{Re}(\text{CO})_3(\text{PTO})\text{Br}$  fall in those of CBP, which means that the possibility of charge trapping energy transfer path cannot be neglected. To confirm the energy transfer mechanism, the current density–voltage characters of the four EL devices with increasing dopant concentrations are shown in Fig. 7. It is observed that the current density increases with increasing dopant concentrations. In other words, the introduction of  $\text{Re}(\text{CO})_3(\text{PTO})\text{Br}$  into CBP film is positive to improve the charge carrier transportation within the EL devices. The oxadiazole moiety in PTO ligand can exhibit some electron transporting character and thus is responsible for the improvement of charge carrier balance. Consequently, the charge trapping energy transfer path should not be responsible

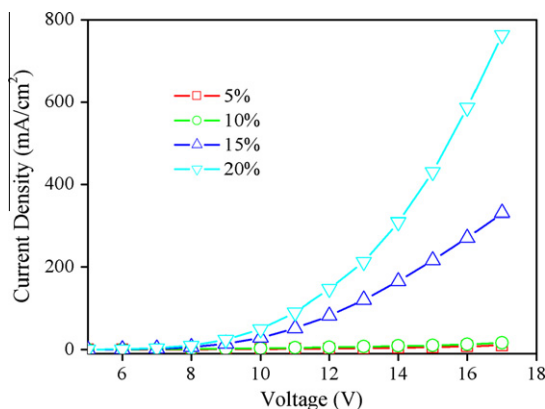


**Fig. 7.** Current density/voltage characteristics of the four devices with increasing dopant concentrations.

for the major energy transfer mechanism. In addition, the EL spectra also suggest that more and more exciton energy has been transferred to  $\text{Re}(\text{CO})_3(\text{PTO})\text{Br}$  emitter with increasing dopant concentration, further confirming the Förster energy transfer mechanism. Then we come to a conclusion that the device performance is compromised by  $\text{Re}(\text{CO})_3(\text{PTO})\text{Br}$ 's low emission yield owing to the electron-withdrawing ligand of PTO [20,21]. However, the electron-withdrawing ligand is positive to shorten the short excited state lifetime, which means that the diamine ligand should be further modified to achieve both short excited state lifetime and high emission yield.

#### 4. Conclusion

In this paper, a novel phosphorescent Re(I) complex of  $\text{Re}(\text{CO})_3(\text{PTO})\text{Br}$  is synthesized and discussed, including its photophysical performance, structural and electronic nature, electrochemical and thermal properties.  $\text{Re}(\text{CO})_3(\text{PTO})\text{Br}$  is found to be a yellow emitter peaking at 549 nm with short excited state lifetime. The Re(I) center localizes in a distorted octahedral field in  $\text{Re}(\text{CO})_3(\text{PTO})\text{Br}$  and the emissive state has MLCT character, leading to the room-temperature phosphorescence. Further analysis reveals that  $\text{Re}(\text{CO})_3(\text{PTO})\text{Br}$  has HOMO and LUMO energy levels at  $-5.79$  V and  $-3.49$  V, respectively, as well as its high thermal decomposition temperature of 322 °C. Using  $\text{Re}(\text{CO})_3(\text{PTO})\text{Br}$  as a dopant, an electroluminescence peaking at 598 nm is realized, with a maximum luminance of 4600  $\text{cd}/\text{m}^2$  and a maximum current efficiency of 11.5  $\text{cd}/\text{A}$ . The low emission yield, however, limits its further application, and future efforts may be devoted to complex structure design and device optimization for performance improvement.

#### Acknowledgment

Project No. CDJZR11 220003 supported by the Fundamental Research Funds of the Central Universities.

#### References

- [1] L. Cambot, M. Cantuel, Y. Leydet, G. Jonusauskas, D.M. Bassani, N.D. McClenaghan, *Coord. Chem. Rev.* 252 (2008) 2572–2584.
- [2] D.V. Scaltrito, D.W. Thompson, J.A. O'Callaghan, G.J. Meyer, *Coord. Chem. Rev.* 208 (2000) 243–266.
- [3] P.T. Furuta, L. Deng, S. Garon, M.E. Thompson, J.M.J. Frechet, *J. Am. Chem. Soc.* 126 (2004) 15388–15389.
- [4] A.S. Ionkin, W.J. Marshall, Y. Wang, *Organometallics* 24 (2005) 619–727.
- [5] M.A. Baldo, D.F. O'Brien, Y. You, A. Shoustikov, S. Sibley, M.E. Thompson, S.R. Forrest, *Nature* 395 (1998) 151–154.

<sup>1</sup> For interpretation of color in Figs. 2–7, the reader is referred to the web version of this article.

- [6] H.Y. Chen, Y. Chi, C.S. Liu, J.K. Yu, Y.M. Cheng, K.S. Chen, P.T. Chou, S.M. Peng, G.H. Lee, A.J. Carty, S.J. Yeh, C.T. Chen, *Adv. Funct. Mater.* 15 (2005) 567–574.
- [7] C. Adachi, M.A. Baldo, S.R. Forrest, S. Lamansky, M.E. Thompson, R.C. Kwong, *Appl. Phys. Lett.* 78 (2001) 1622–1624.
- [8] Z. Si, X. Li, X. Li, H. Zhang, *J. Organomet. Chem.* 694 (2009) 3742–3748.
- [9] X. Li, D. Zhang, W. Li, B. Chu, L. Han, T. Li, Z. Su, J. Zhu, Y. Chen, Z. Hu, P. Lei, Z. Zhang, *Opt. Mater.* 31 (2009) 1173–1176.
- [10] X. Li, X. Liu, Z. Wu, H. Zhang, *J. Phys. Chem. A* 112 (2008) 11190–11197.
- [11] L. Shi, B. Li, S. Yue, D. Fan, *Sensor Actuat. B Chem.* 137 (2009) 386–392.
- [12] Y. Wang, H.J. Mao, G.Q. Zang, Y.S. Yu, Z.H. Tang, *Spectrochim. Acta A* 78 (2011) 469–473.
- [13] L. Yang, J.K. Feng, A.M. Ren, M. Zhang, Y.G. Ma, X.D. Liu, *Eur. J. Inorg. Chem.* 10 (2005) 1867–1879.
- [14] L. Zhang, B. Li, Z. Su, *Langmuir* 25 (2009) 2068–2074.
- [15] L. Zhang, B. Li, *J. Lumin.* 129 (2009) 1304–1308.
- [16] L. Zhang, B. Li, *J. Electrochem. Soc.* 156 (2009) J174–J178.
- [17] G.B. Che, Z.S. Su, W.L. Li, B. Chu, M.T. Li, *Appl. Phys. Lett.* 89 (2006) 103511–103513.
- [18] L. Zhang, P. Chen, B. Li, Z. Hong, S. Liu, *J. Phys. D: Appl. Phys.* 41 (2008) 245101–245113.
- [19] M.A. Baldo, C. Adachi, S.R. Forrest, *Phys. Rev. B* 62 (2000) 10967–10977.
- [20] Z. Si, J. Li, B. Li, F. Zhao, S. Liu, W. Li, *Inorg. Chem.* 46 (2007) 6155–6163.
- [21] C.B. Liu, J. Li, B. Li, Z.R. Hong, F.F. Zhao, S.Y. Liu, W.L. Li, *Appl. Phys. Lett.* 89 (2006) 243511–243513.